

Learning to Dehaze From Realistic Scene with A Fast Physics-based Dehazing Network

Ruoteng Li, *Member, IEEE*, Xiaoyi Zhang, Shaodi You, *Member, IEEE*, and Yu Li, *Member, IEEE*

Abstract—Dehazing is a popular computer vision topic for long. A real-time dehazing method with reliable performance is highly desired for many applications such as autonomous driving. While recent learning-based methods require datasets containing pairs of hazy images and clean ground truth references, it is generally impossible to capture accurate ground truth in real scenes. Many existing works compromise this difficulty to generate hazy images by rendering the haze from depth on common RGBD datasets using the haze imaging model. However, there is still a gap between the synthetic datasets and real hazy images as large datasets with high-quality depth are mostly indoor and depth maps for outdoor are imprecise. In this paper, we complement the existing datasets with a new, large, and diverse dehazing dataset containing real outdoor scenes from High-Definition (HD) 3D movies. We select a large number of high-quality frames of real outdoor scenes and render haze on them using depth from stereo. Our dataset is more realistic than existing ones and we demonstrate that using this dataset greatly improves the dehazing performance on real scenes. In addition to the dataset, we also propose a light and reliable dehazing network inspired by the physics model. Our approach outperforms other methods by a large margin and becomes the new state-of-the-art method. Moreover, the light-weight design of the network enables our method to run at a real-time speed, which is much faster than other baseline methods.

I. INTRODUCTION

Haze is one of the most common bad weather phenomena caused by floating atmospheric particles that degrade the contrast and visibility of images captured outside. Many vision-based algorithms deployed in outdoor environment suffer from hazy conditions such as object detection [1]. It is important to enhance the visibility of hazy images so as to boost the performance of various important computer vision tasks.

Since the first single image dehazing work in 2008 [2], a large number of haze removal methods have been proposed [3], [4], [5]. Unlike traditional model-based dehazing algorithms, data driven methods proposed in recent years require the training datasets with high quality ground truth. To that end, a number of dehazing datasets are proposed, most of which are synthetic datasets rendered based on the optical model for particle scattering known as Koschmieder’s law [6]. The light luminance \mathbf{I} captured at a certain pixel $\mathbf{x} = (x, y)$ can be expressed as:

$$\mathbf{I}(\mathbf{x}) = \mathbf{J}(\mathbf{x})e^{-\beta d(\mathbf{x})} + \mathbf{A}(1 - e^{-\beta d(\mathbf{x})}), \quad (1)$$

R. Li and X. Zhang are with the Department of Electrical and computer Engineering, National University of Singapore. E-mail: {liruoteng, zhangxiaoyi}@u.nus.edu

S. You is with University of Amsterdam, Amsterdam, Netherlands E-mail: s.you@uva.nl

Y. Li is with Applied Research Center, Tencent PCG and University of Illinois Urbana-Champaign, IL, US, E-mail: ianyli@tencent.com

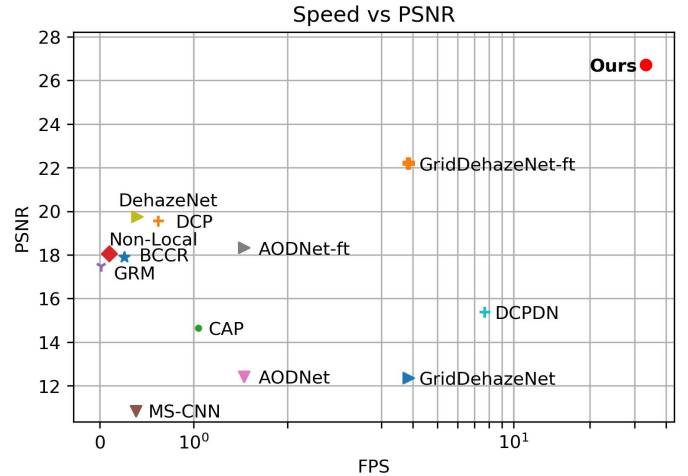


Fig. 1: The speed (FPS) v.s. accuracy (PSNR) comparison on our new realistic dehazing dataset with resolution 460×620 . The proposed method achieves the best performance and remains the fastest processing speed among all the baseline methods. See more details in Sec. V.

where \mathbf{J} represents the light emitted from the scene object, attenuated by the scattering media with a coefficient $e^{-\beta d(\mathbf{x})}$. $d(\mathbf{x})$ represents the absolute depth value at location \mathbf{x} . \mathbf{A} is the atmospheric light. Physically, the degradation in hazy images can be attributed to floating particles that absorb and scatter light in the environment [6]. This scattering and absorption reduces the direct transmission from the scene to the camera and adds another layer of the scattered light, known as airlight [7]. The attenuated direct transmission causes the intensity from the scene to be weaker, while the airlight causes the appearance of the scene to be washed out.

Most of the existing dehazing datasets render images based on Eq. (1). Generally, the rendering pipeline requires accurate depth information $d(\mathbf{x})$ of the scenes. However, it is usually very difficult to obtain accurate and dense depth maps from outdoor scenes. Some of the existing datasets collect RGBD images with the aid of infrared information [4], but infrared is usually lack of accuracy in wild outdoor scenes. Other datasets apply the latest depth estimation algorithms. However, depth estimation algorithms do not provide high quality scene depth because depth estimation itself is still an open research topic.

In this paper, we argue two important bottlenecks of single image dehazing:

- A large-scale high-quality and realistic dataset is required for current dehazing algorithm. Especially, accurate and

physically-valid ground truth is crucial for effectively training a dehazing method.

- A network that can work in real-time and with efficient power and memory usage is desired for real applications. This network can be widely applied to a lot of resource constraint and dynamic outdoor scenarios, such as autonomous cars, UAV, and underwater robots.

First, existing synthetic datasets suffer from unrealistic haze and inaccurate ground truth as shown in Fig. 2. Some of the datasets (*e.g.*, [3], [5] and [8]) contain only dozens of samples, which are not enough for learning-based methods. Although the dataset proposed by [4] is large-scale, the synthetic haze is rendered on indoor scenes, which differs from the real-world scenarios. In addition, the outdoor subset of [4] applies monocular depth estimation to obtain the depth. However, the estimated depth is neither physically valid nor accurate, causing the rendered hazy images not realistic.

Second, as illustrated in Fig. 1, while we find most of the existing methods demonstrate a satisfying performance in terms of PSNR, their networks are computationally expensive and cannot be properly applied to outdoor mobile vehicles, such as UAVs, small sized robots and low end autonomous cars. It can also be found that most of the existing networks run only at 3 frames per second (FPS) or slower, which is not satisfied for real-time applications.

We aim to tackle both of the aforementioned problems through physics inspiration. Based on the physics modeling, we first propose a large, high quality, highly various dataset. For building this dataset, we select 2000 high quality ground truth images from 3D movies with a 1920×1080 resolution. The images are captured by high end cameras where the color, exposure, and sensor noise are optimized. The 2000 ground truth images are from 22 different movies with 40 hours in total to ensure their diversity. More importantly, all those movies are captured by multi-view stereo cameras, so that we can obtain high quality depth that enables us to render the high quality and physics realistic hazy images. Fig. 2 shows some examples and comparisons with existing datasets. Details of the dataset creation are described in Sec. III.

Third, inspired by the physics model, we propose a light-weight and reliable neural network. Particularly, the proposed network contains two stages. The first stage incorporates the physics model to estimate the transmission map and the atmospheric light. With the guidance of the transmission map and the atmospheric light, the second stage learns to recover the clean background image from the output of previous stage and the hazy input image. The proposed network is simple, fast and accurate as shown in the experiment section. Fig. 1 shows the performance of our proposed network. Details of the network structure and the implementation is described in Sec. IV.

Finally, this paper propose a systematical and a detailed benchmark using the proposed dataset and existing datasets. We believe this work will enable more exciting and novel topics in dehazing. Moreover, we also demonstrate the state-of-the-art performance of the proposed network.

The main contributions of this paper can be summarized as:

- We create a large-scale, high-quality, physically-valid outdoor dehazing dataset of real scenes.
- We propose an efficient and high performance dehazing network based on physics inspiration, which can be applied to various real-time dynamic and resource constraint outdoor scenes. Rigorous experiments demonstrate the state-of-the-art efficiency and accuracy of the proposed network.
- We provide a systematical benchmark of existing methods on both the existing RESIDE [4] dataset and the proposed dataset.

II. RELATED WORK

Haze removal from a single image has attracted wide attention. Some research works on dehazing require multiple images (*e.g.* [10], [11]) or additional information from other sources (*e.g.* [12], [13]). A comprehensive survey for dehazing can be found in [8]. In this work, we only focus on single image dehazing.

Single image dehazing methods Early works on single image dehazing are mostly prior based. These works propose different priors in estimating the transmission map and the air light and then a clean image can be recovered by reversing the hazy image model in Eq. 1. Tan *et al.* [2] proposes to use local contrast maximization and [9] uses the idea that the shading and transmission functions are locally and statistically uncorrelated. [14], [15] observe an interesting phenomenon of outdoor natural scenes with clear visibility and formulate as dark channel prior (DCP), which becomes one of the most successful priors to dehaze. [16] extends the idea of the dark channel prior in determining the initial values of transmission by the boundary constraints and refines the map by a contextual regularization. [17] gathers multiple and multi-scale features from existing priors and uses a random forest regressor to learn to predict the transmission from the features. [18] introduces a color attenuation prior and create a linear model for scene depth, where the parameters of the model are learned in a supervised learning fashion. Unlike the previous patch-based priors, the work of [19] develops a non-local prior which relies on the assumption that colors of a haze-free image form tight clusters in RGB space. [20] proposes to use optimization to solve the dehazing and in the meanwhile minimizing the visual artifacts [21]. [22] links the traditional Retinex methods to the dehazing problem. Some researches address more specific problems, *e.g.* atmospheric light estimation [23] and nighttime dehazing [24], [25].

With the advance of deep learning technologies and their success in many computer vision applications, convolution neural network (CNN) based methods for image dehazing gain increasing popularity in recent years [22], [26], [27], [28], [29], [30], [31], [32], [33], [34], [35], [36]. Unlike prior based methods that rely on hand-crafted features, the CNN based methods try to learn the dehazing features directly from the training data. DehazeNet [26] trains a CNN to predict the transmission value at local patches. [33] proposes to use multi-scale CNN (MSCNN) to first generate a coarse transmission map and gradually refine it. The All-in-One

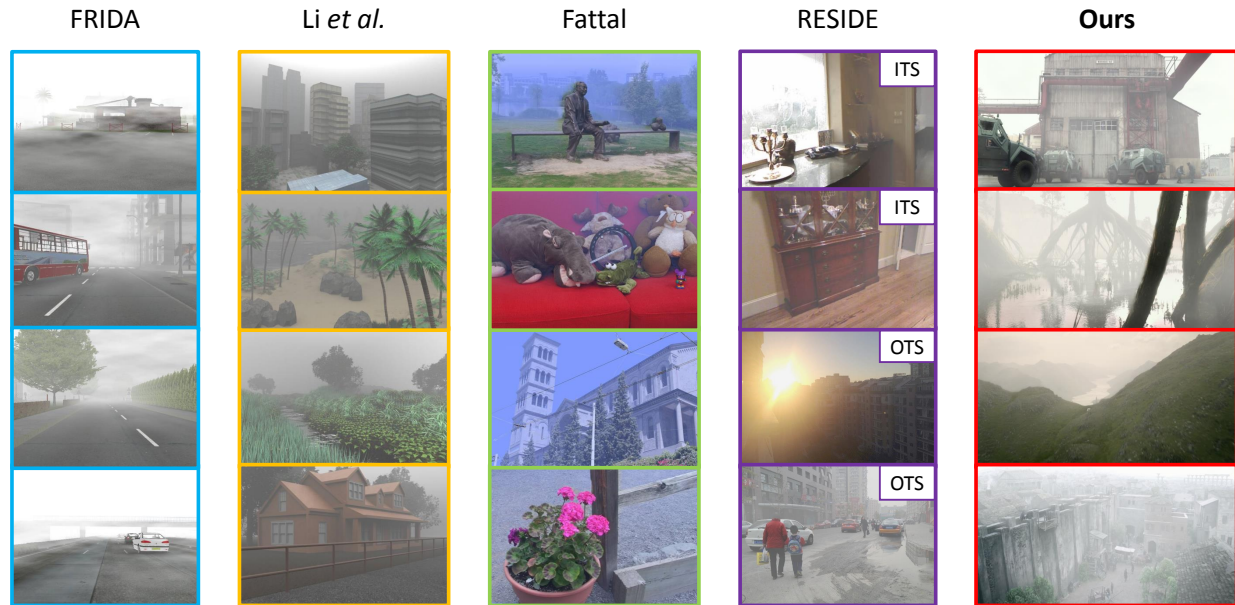


Fig. 2: A visual comparison of the existing datasets including Frida [5], Li *et al.* [8], Fattal [9], RESIDE [4], and our proposed dataset. ITS and OTS indicate indoor training set and outdoor training set respectively.

Dehazing Network (AODNet) [27] re-writes the scattering model to enable a network to generate clean image directly without explicitly estimating the transmission and atmosphere light separately. [36] trains a Densely Connected Pyramid Dehazing Network (DCPDN) with an edge-preserving loss and introduces a discriminator in dehazing. Methods [34], [35] incorporate traditional dehazing priors and color processing operations into the deep network. Generative adversarial network (GAN) based dehazing methods have been proposed in [28], [32]. The recent state-of-the-art method [30] applies a novel attention-based multi-scale estimation on a grid network.

Dehazing datasets Quantitative evaluation for dehazing requires the hazy image and the corresponding clean background as a reference. These pairs are generally difficult to capture in real as it is usually impossible to control the outdoor environments. Researchers in this field find other ways for generating the datasets. The most common approach is to render haze on clean images with its depth information using Eq. 1 [3], [4], [5]. An exception is the dataset of Li *et al.* [8] that applies physics-based rendering technique (*i.e.* ray tracing) [37] to generate the haze effect on synthetic scenes. Fattal [3] provides a dehazing dataset rendered from real images and their depth maps. FRIDA [5] dataset focuses on driving scenarios and uses synthetic road backgrounds from graphics models. These early datasets are all limited in size and can serve only as small benchmarking. To meet the need for training a neural network for dehazing, large scale datasets are then created. [38] introduces a foggy Cityscapes dataset using images from the Cityscapes dataset [39]. [4] proposes a general dehazing dataset named RESIDE. Its indoor training set (ITS) is built on existing indoor RGBD datasets NYUv2 [40] and Middlebury

stereo [41]. The outdoor training set (OTS) collects real outdoor images with their depth estimated using [42]. Other kinds of datasets like subjective evaluation datasets and task-driven datasets are not discussed here.

III. LARGE-SCALE REAL OUTDOOR DATASET

In this section, we introduce the details of our large-scale high-quality real outdoor dataset. We call it large-scale Fine Depth dehazing dataset, **LSFD** dataset for short.

A. Dataset Overview

The proposed dehazing dataset contains a total of 10000 images, of which 8000 images are for training set and the rest 2000 images belong to the test set. The hazy images are rendered on 2000 high-quality clean images, extracted from a series of High-Definition (HD) 3D movies. In order to diversify the background scenes, we extract around 100 key frame-pairs from each of totally 22 movies and render 5 hazy images on each clean background frame with various haze densities. For the training set, each sample contains four items including the rendered hazy image I , the transmission map T , the atmospheric light value A and the corresponding clean background image C . In the following sections, we will explain clean image selection, image depth generation, and hazy image rendering process in detail.

B. Outdoor Image Data

We have listed the comparison of all the existing general dehazing datasets in Table I. Note Sakaridis [38] dataset focuses specifically on semantic scene understanding for the driving

TABLE I: Comparison of the proposed dataset with existing dehazing datasets. The proposed dataset contains the most diverse and accurate depth.

	Indoor	Outdoor	Background	Diversity	Haze effect	Depth accuracy
Fattal [3]	4	8	Real	Low	Using depth	High
FRIDA [5]	-	480	Synthetic	Low	Using depth	High
Li <i>et al.</i> [8]	-	5	Synthetic	Low	Ray tracing	-
RESIDE-ITS [4]	1399	-	Real	Low	Using depth	High
RESIDE-OTS [4]	-	2061	Real	High	Using depth	Low
Ours	-	2000	Real	High	Using depth	High

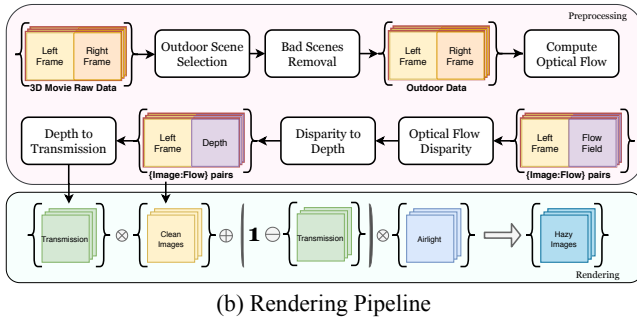
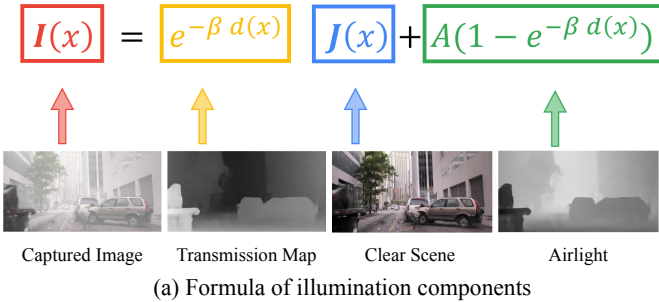


Fig. 3: Illustration of the hazy image model and visibility degradation effect. It can be found that the image visibility is degraded mainly from two aspects: the light scattering and the color shifting. We can observe that the distant area are less visible due to the light absorption. Moreover, the color tone is shifted towards the airlight due to the light scattering.

scenes, which is not listed. From the table, we can see that most of the early datasets contain a limited number of samples, which are not suitable for data-driven methods. Existing large-scale outdoor dehazing dataset, *i.e.* the "RESIDE- β " dataset [4], is rendered based on monocular depth estimation [42]. However, monocular depth estimation is not reliable and not physically valid. Especially, the depth estimation method used to generate the transmission map does not perform reliably at many texture-less and ambiguous areas [43]. To overcome the limitation of single image depth estimation, we consider utilizing a stereo algorithm to provide robust and accurate outdoor depth. We find that 3D movies provide the largest known source of stereo pairs, presenting the possibility of capturing millions of outdoor scenes with stereo information available. Thus, we propose to extract depth data from 3D movies. In recent times, high-quality 3D movies are usually captured by top-notch stereo cameras and feature diverse and

dynamic environments that range from human-centric imagery (such as Hollywood films) to nature scenes with landscapes and animals in scientific documentaries. To that end, we select a diverse set of 22 recent 3D movies with stereo image-pairs available.

C. 3D Movies Pre-processing

Outdoor Scene Selection In order to obtain rich and diverse outdoor scenes data with stereo camera settings, we carefully select a series of 3D movies that provide a large number of high-quality stereo pairs in controlled conditions. In a typical 2-hour modern movie, the video may contain up to hundreds of different clips including both indoor and outdoor scenes. In order to obtain consecutive frames in the same scene, we split the long video into individual segments separated by scene transitions. To that end, we apply an existing scene detection algorithm [44] to split each movie into independent clips, each of which contains a movie segment recorded under the same scene. For each segment, we extract up to 2 frames (image pairs) as clean background images. These two frames are selected from the first and the last of the segment respectively to ensure considerable camera motion. All the extracted frames form the image set S_0 . From set S_0 , we then apply the state-of-the-art semantic segmentation method [45] to select outdoor images to form image set S_1 . In order to make sure the selected scenes are from outdoor environments, we only select the images with common outdoor semantic objects including grassland, road, building, landscape, *etc.*. Lastly, not all the images from S_1 are useful for haze rendering because of various reasons. Some of the scenes are recorded under foggy, hazy, or smoky conditions. Others may contain strong motion blur or de-focus blur. For this, we manually check the image set S_1 to exclude blurry images, low-light or dark images, texture-less images, foggy or hazy backgrounds, science-fiction style unnatural images, *etc.*. After these procedures, We obtain the final set of images as ground truth data for haze rendering.

Depth Map An accurate depth map of a scene is the key to make a high-quality dehazing dataset useful. However, the depth maps in outdoor scenes are extremely difficult to obtain. Existing dehazing datasets use either [42] depth estimation algorithm [4] or semantic annotations [38] to obtain coarse depth maps. Their depth maps do not have satisfying accuracy as shown in Fig. 5. In contrast, our dataset has more accurate depth maps for haze rendering by using stereo camera images.

Although 3D movies provide stereo image pairs for every frame, the movie data comes with its own issues as well. First,



Fig. 4: Some samples of the proposed dataset. The airlight are generated in consistent with the color tone of the background image.

some 3D films are shot with monocular cameras and the stereo effects are manually added by post-processing. In this case, we only select movies that were shot using physical stereo cameras. Second, we only select Blu-ray format high definition movies, which allow us to make high-resolution images. In addition, camera focal lengths, stereo camera baselines, and camera intrinsic parameters are usually unknown and these parameters vary from one movie to another. It is difficult to directly compute the stereo disparity solely from the image pairs using the state-of-the-art stereo estimation algorithms. In addition, most of the stereo algorithms are designed and trained to estimate disparity in positive ranges only. However, the 3D movie data may contain negative disparity values because of the camera rotation in the stereo rig configuration. Instead of applying stereo algorithms, we apply the state-of-the-art optical flow estimation method PWCNet [46] to handle the positive and negative disparity values. We only retain the horizontal component of the flow field as the disparity.

Depth Map Refinement The PWCNet [46] produces flow fields in a quarter of the original image size. A bi-linear up-sampling post-processing is usually used to up-sample the flow fields to the full size. In our case, the bi-linear up-

sampling usually makes the object’s boundary blurry (shown in Fig. 5), which also leads to halo effect on the rendered object’s boundary. To solve this, we apply FGI [47] algorithm to up-sample the flow fields based on the boundary, contours, and edges of the input image. Fig. 5 compares the depth maps of these two up-sampling methods. We can observe that the depth discontinuities are more aligned with the actual objects’ boundaries in the input images. Hence, the halo effects of the FGI up-sampled results are significantly reduced.

D. Haze Rendering

Our rendering follows the haze model [26], [22], [27], [28] described in Eq. 1. The detailed rendering process is described in Algorithm 1. For each clean background image, we synthesize 5 hazy images using different β values uniformly sampled from [1.0, 3.0], resulting in 10000 hazy images. 8000 hazy images are split into training set and the rest 2000 images are for the test set.

The atmospheric light value \mathbf{A} is determined using maximum color method described in Eq.(2).

$$A_C = \max_{\mathbf{x} \in I} C(\mathbf{x}), C = R, G, B, \quad (2)$$

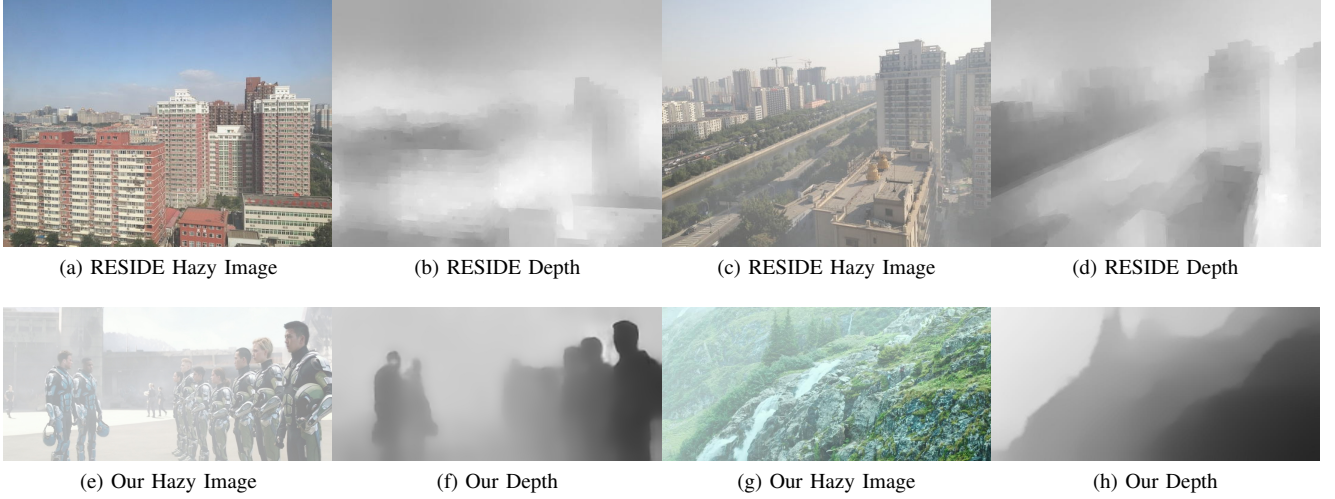


Fig. 5: Depth map comparison between the proposed dataset with RESIDE- β [4].

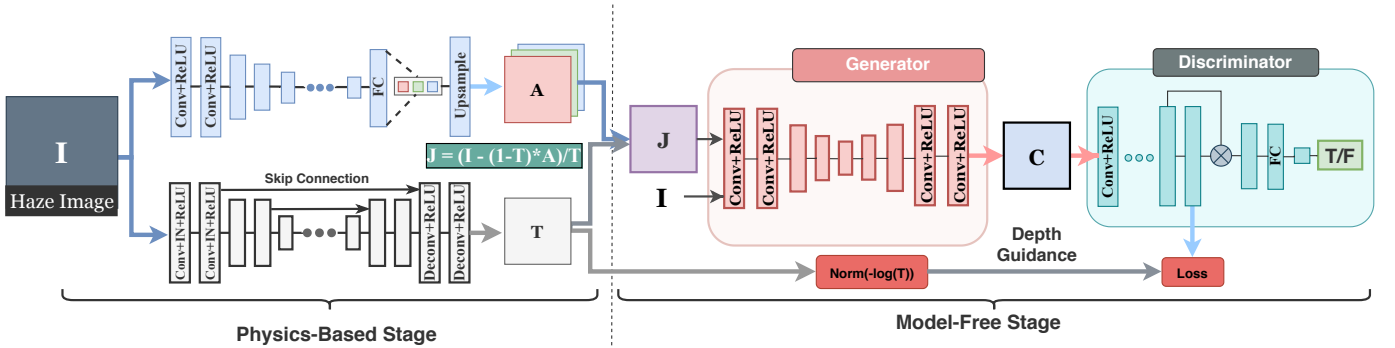


Fig. 6: The architecture of the proposed dehazing network. In the first stage, the network learns the atmospheric light and transmission. The second stage of the network learns to recover the clean background image.

which is widely used in white balance. The airlight needs to be consistent with the environment lighting in the haze free image. Since we are using movie images for the haze free image, the lighting and color tone are usually adjusted from there natural exposure. Therefore, we need to adjust the airlight accordingly.

IV. PHYSICS INSPIRED EFFICIENT DEHAZING NETWORK

Along with the proposed large-scale realistic dataset, we also propose a light-weight two-stage dehazing network to show that the proposed dataset has better generalization than the existing dehazing datasets. We also argue that the physics modeling allows us to develop a network that is fast and light, which is essential for online visibility enhancement.

The overall architecture of the proposed method is shown in Fig. 6. Before describing the proposed 2-stage network, we first discuss the overall input and output of the network, as well as the intermediate output of the first stage. Referring to Fig. 6, we call the first stage as the physics-based network. It takes in a single hazy image as input and extracts the physical parameters of haze, including the transmission map T and the atmospheric light A . The output of this first stage is the clean

background image J , which is reconstructed by the following equation:

$$J = \frac{I - (1 - T) \odot A}{T}. \quad (3)$$

In the second stage, we construct a basic conditional generative adversarial network (cGAN) to refine the output image J . The generative network takes in the reconstructed image J as well as the predicted transmission T and predicted atmospheric light A , and produces the refined clean image C . The discriminative network is used to determine whether this is a real clean image. Hence, the refinement network directly learns to map the reconstructed image J to clean images.

Most of the existing networks do not generalize very well when trained on a particular dataset and tested on other data from a different domain. (i.e. train a network on synthetic data and test it on real data). For this reason, we should add another refinement network, the model-free network, which does not assume any hand-crafted model. Hence, unlike the first stage, the refinement network is not guided by the proposed equation but directly learns the transfer function from the hazy images to clean images.

A. Physics-based Stage

The physics-based stage of the proposed network contains two branches. The first branch is for atmospheric light estimation, called AtmNet (shown in Fig. 6 top). Another branch is a transmission estimation sub-network called TransNet (shown in Fig. 6 bottom).

Learning Atmospheric Light \mathbf{A} The AtmNet learns to predict the global atmospheric light from the input hazy images. This sub-network is composed of 5 Conv+ReLU blocks appended with 2 fully-connected layers. The output \mathbf{A} from the second fully-connected layer is a three-value vector indicating RGB color channels. \mathbf{A} is then up-sampled to the size of the input image. The loss function for learning atmospheric light \mathbf{A} is defined as:

$$\mathcal{L}_A = \mathcal{L}_{MSE}(\mathbf{A}, \mathbf{A}_{gt}), \quad (4)$$

where \mathbf{A}_{gt} is the ground truth of the atmospheric light and \mathbf{A} is the predicted atmospheric light map. The loss function \mathcal{L}_{MSE} computes the mean-square-error between the predicted \mathbf{A} and the ground truth \mathbf{A}_{gt} .

Learning Transmission Map Transmission map encodes the global depth information of a scene [30]. To learn the global transmission map well, we use an auto-encoder with dilated convolution to provide the network larger with receptive fields. Instead of using batch normalization, we adopt the instance normalization [48] in the first two convolutional layers in our experiments because the batch normalization usually performs poorly when the testing data is from a different domain. The loss function for learning the transmission map \mathbf{T} is defined as:

$$\mathcal{L}_T = \mathcal{L}_{MSE}(\mathbf{T}, \mathbf{T}_{gt}). \quad (5)$$

B. Refinement Stage

The model-free refinement stage contains a conditional generative adversarial network. The generative network takes the estimated image \mathbf{J} and fog image \mathbf{I} as the input. The goal of the generative network is to generate a refined and cleaner version \mathbf{C} that are visually appealing and free from the fog effect and the artefacts produced by the previous stage. The input of this generator is the concatenated results of the reconstructed image \mathbf{J} , predicted transmission map \mathbf{T} , the predicted atmospheric light \mathbf{A} , and the input image \mathbf{I} . We minimize the Mean-Square-Error (MSE) loss and perceptual loss [49] to train the generative network and the full loss function is formulated as:

$$\begin{aligned} \mathcal{L}_C = & \mathcal{L}_{MSE}(\mathbf{C}, \mathbf{C}_{gt}) \\ & + \lambda_p \mathcal{L}_{MSE}(VGG(\mathbf{C}), VGG(\mathbf{C}_{gt})), \end{aligned}$$

where λ_p represents the weighting term between the MSE loss and perceptual loss. In this work, we set it to 1. VGG represents the VGG16 [50] network pretrained on the ImageNet dataset [51].

Overall, the loss function for the generative network is formulated as follows:

$$\mathcal{L}_G = \mathcal{L}_C + \lambda_{GAN} \mathcal{L}_{GAN}(C), \quad (6)$$

Algorithm 1 Proposed Haze Rendering

- 1: **Input:** Clean Image \mathbf{C} and its depth map \mathbf{d}
- 2: $\mathbf{C}_{blur}(\mathbf{x}) = \text{imgaussfilt}(\mathbf{C}(\mathbf{x}), \sigma_{\mathbf{C}}(\mathbf{x}))$. The smooth kernel varies according to depth: $\sigma_{\mathbf{C}}(\mathbf{x}) = 1.5\mathbf{d}(\mathbf{x})$.
- 3: Obtain Transmission $\mathbf{T} = \exp^{-\beta\mathbf{d}}$, $\beta \sim U(1, 2.5)$
- 4: Obtain $\mathbf{T}_{blur} = \text{guidedfilt}(\mathbf{T}, \mathbf{T}, \sigma_T)$, $\sigma_T \sim \mathcal{N}(4, 1.0)$.
- 5: Obtain global atmospheric light $\mathbf{A} \sim U(0.3, 0.8)$
- 6: **Output:** Hazy Image $\mathbf{I} = \mathbf{T}_{blur}\mathbf{C} + (1 - \mathbf{T}_{blur})\mathbf{A}$

TABLE II: The quantitative comparison between our method and baseline methods on the proposed dataset *test* set. **ft** indicates the models whose weights are fine-tuned on our dataset, otherwise the official weights of the models are used. The upper five methods are traditional dehazing methods and the rest are CNN-based methods.

Methods	PSNR	SSIM
BCCR [16]	17.91	0.729
DCP [15]	19.56	0.761
CAP [18]	14.64	0.715
Non-Local [19]	18.06	0.727
GRM [20]	17.48	0.682
MS-CNN [33]	10.85	0.687
AODnet [27]	12.42	0.639
AODnet-ft [27]	18.33	0.728
DehazeNet [26]	19.76	0.788
DCPDN [36]	15.38	0.660
GridDehazeNet [30]	12.37	0.659
GridDehazeNet-ft [30]	22.19	0.837
Ours	26.71	0.923

where \mathcal{L}_{GAN} is the adversarial loss and hence $\mathcal{L}_{GAN}(\mathbf{C}) = \log(1 - D(\mathbf{C}))$ and the weighting parameters λ_{GAN} is set to 0.01 in our experiments.

C. Implementation

The proposed network is firstly trained in a stage-wise manner and then fine-tuned on an end-to-end basis. The first physics-based stage is trained on the proposed dataset, to learn transmission and atmospheric light estimation. We use Adam [52] optimizer with weight decay of 10^{-4} and only supervise the loss \mathcal{L}_T and \mathcal{L}_A . The learning rate is set to 0.001 initially and is divided by 2 after every 10 epochs until the 50th epoch. When training the second stage, we fix the learnable parameters of the first stage and only update the refinement sub-network with a comparatively smaller learning rate, starting from 0.0005. The optimizer for training the second network is the same. It is trained from 50th epoch to 100th epoch. The entire network is implemented in PyTorch framework and is processed on NVIDIA GTX1080 Ti GPU. The overall training time is approximately 24 hours.

V. BENCHMARK

In this section, we evaluate our algorithm and compare it with the popular conventional methods and recent CNN based methods. The traditional dehazing methods tested include Boundary Constrained Context Regularization (BCCR) [16], Color Attenuation Prior (CAP) [18], Dark-Channel Prior



Fig. 7: Results comparison on the proposed dataset.

(DCP) [15], Artifact Suppression via Gradient Residual Minimization (GRM) [20], and Non-local Image Dehazing (non-local) [19]. For CNN-based methods, we evaluate DehazeNet [26], Multi-scale CNN (MSCNN) [33], All-in-One Dehazing (AODNet) [27], Densely Connected Pyramid Dehazing Network (DCPDN) [36], and grid [30]. We present the evaluation results on our proposed dataset on Table II and the most recent dehazing dataset *Reside*[4] on Table III.

A. Results on the Proposed Dataset

We first evaluate the traditional dehazing algorithms and the CNN-based methods on the proposed datasets as shown

in Table II. We use PSNR [53] and SSIM [54] metrics to evaluate all the methods. The conventional methods are directly applied on the proposed test set. For CNN-based methods, we directly use the weights provided by the author to test on the proposed datasets. From the table, we can see that the proposed method outperforms other methods for both PSNR and SSIM evaluations. Since the proposed method contains comparatively denser haze, the CNN-based baseline methods could not perform well since most of the methods are single-stage, which are not designed for dense haze conditions. The conventional dehazing algorithms tend to make the background darker and over saturated as shown in Fig. 7 and 8.

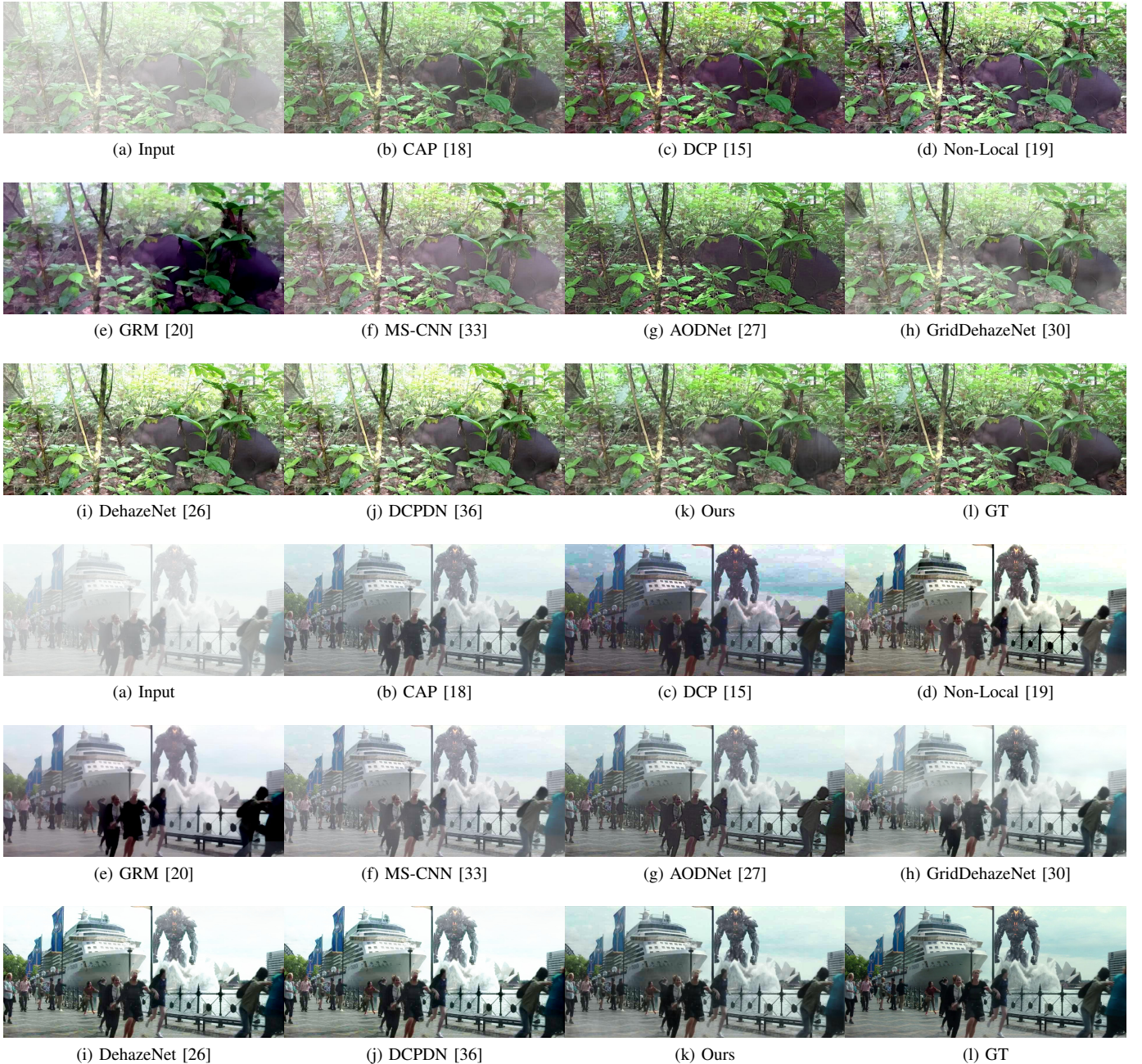


Fig. 8: Results comparison on the proposed dataset.

From the figures, we may also find that baseline methods [33], [30] tend to predict wrong depth at some objects. However, the proposed method is able to predict appropriate depth value and object depth boundaries.

B. Results on RESIDE- β dataset

We finetune our network on the training set of RESIDE[28] and test it on the test set. The results are shown in Fig. 10. Since the RESIDE dataset renders comparatively light haze and the transmission maps do not align with the actual background depth well. We may observe that most of the CNN methods cannot perform well on this test data. The

atmospheric light estimation plays an important role for the conventional baseline methods. GRM [20] and AODNet[27] reveal poor performance because of the inaccurate estimation (implicit) on atmospheric light. Therefore the color in the results deviates from the ground truth.

C. Running time on test images

The running time comparisons of our proposed network and other baseline methods are shown in the last column of Table III. The running time testing setup follows [4]. The time is average over running the synthetic indoor images of size 620×460 in the synthetic indoor testing sets. For CPU

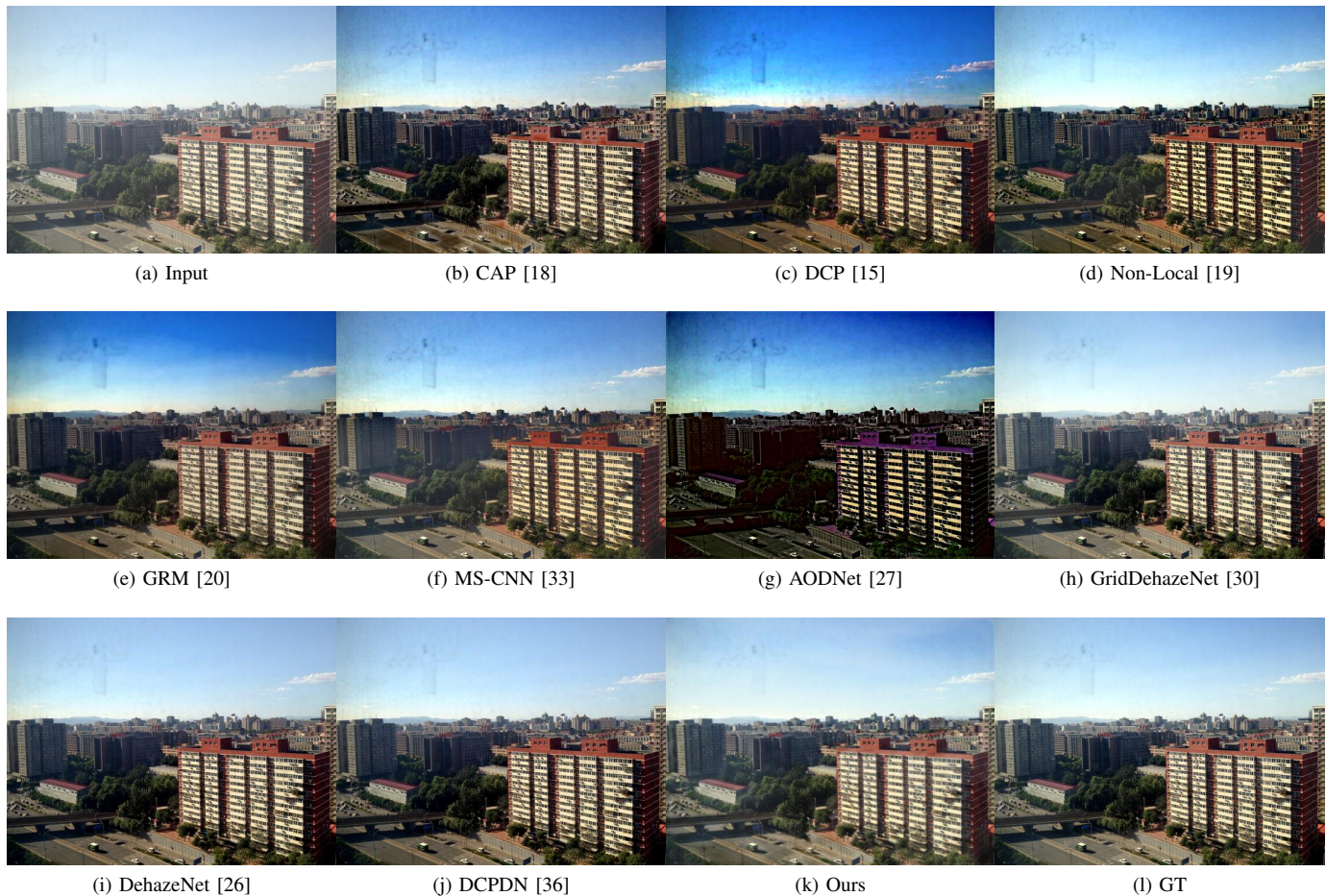


Fig. 9: Results comparison on RESIDE- β [4] dataset.

TABLE III: The quantitative comparison between our method and baseline methods on RESIDE [4] dataset.

Methods	PSNR	SSIM	Time (s)
BCCR [16]	16.88	0.7913	3.85
DCP [15]	16.62	16.62	1.62
CAP [18]	19.05	0.8364	0.95
Non-Local [19]	17.29	0.7489	9.89
GRM [20]	18.86	0.8553	83.96
MS-CNN [33]	17.57	0.8102	2.60
AODnet [27]	19.06	0.8504	0.65
DehazeNet [26]	21.14	0.8472	2.51
GridDehazeNet [30]	30.86	0.9819	0.26
Ours	30.33	0.9473	0.03

algorithms [16], [18], [15], [20], [19] and AOD-Net [27], we quote the reported results in [4]. For GPU algorithms, we test them on a machine with NVIDIA GTX1080 Ti GPU. We can see that our method is about two magnitude faster than the existing methods due to the light-weight design of our network. The two-stage network is able to maintain good performance while working in real-time.

D. Ablation Study

Effectiveness of the refinement network In our proposed method, the dehazing network contains two stages: reconstruct-

tion and refinement. To verify the necessity and effectiveness of the stages, we conduct an ablation study to compare the restore results between the final output C and the intermediate reconstructed result J . The qualitative results on the proposed dataset are shown in Fig.11. From the figures, we can find that the intermediate reconstructed image J is very sensitive to the estimation of atmospheric light A and inaccurate A will result in dark result of the reconstructed image J .

Categorical analysis of the proposed dataset For in depth analysis, in order to provide a deep analysis on the proposed dataset, we divide our dataset into different categories based on the type of the scenes, including *Cityscape*, *Landscape*, *Natural rural* scenes. Besides, we also divide the test sets into Human-centric and non-Human categories. We then test all the existing methods as well as the proposed method on these different categories. The results are shown in Table IV. From the table, we can see that our proposed method consistently outperforms others under all the categories.

It is also interesting to check the performance in different fog densities. For this, we divide the test sets based on the fog density β into 5 different levels. As shown in Table V, the proposed method also outperforms other methods significantly.

TABLE IV: The quantitative comparison between our method and baseline methods on the proposed dataset.

Method	Humancentric		Non-Human		Cityscapes		Landscapes		Natural rural	
	PSNR	SSIM	PSNR	SSIM	PSNR	SSIM	PSNR	SSIM	PSNR	SSIM
BCCR [16]	17.93	0.7242	18.04	0.7403	18.03	0.7397	17.88	0.7369	18.04	0.7575
DCP [15]	19.62	0.7546	19.52	0.7702	19.18	0.7616	19.70	0.7710	19.83	0.7948
CAP [18]	14.21	0.6991	15.07	0.7300	14.85	0.7272	14.59	0.7185	15.08	0.73985
Non-Local [19]	17.53	0.7075	18.38	0.7430	18.02	0.7344	18.38	0.7405	18.64	0.7537
GRM [20]	17.28	0.6671	17.64	0.6960	17.63	0.6899	17.70	0.7021	17.76	0.7075
AODnet [27]	18.49	0.6997	18.71	0.7486	18.53	0.7362	18.48	0.7369	18.68	0.7772
GridDehazeNet [30]	22.45	0.8110	22.58	0.8539	22.17	0.8414	22.44	0.8501	23.07	0.8832
Ours	25.81	0.9037	25.91	0.9126	26.16	0.9142	26.47	0.9168	25.98	0.9213

TABLE V: The quantitative comparison between our method and baseline methods on the proposed dataset with different haze/fog densities β .

Method	$\beta = 1.5$		$\beta = 1.4$		$\beta = 1.3$		$\beta = 1.2$		$\beta = 1.1$	
	PSNR	SSIM								
BCCR [16]	17.95	0.7333	17.85	0.7299	17.77	0.7175	17.99	0.7279	18.05	0.7376
DCP [15]	19.80	0.7704	19.65	0.7641	19.59	0.7507	19.32	0.7556	19.53	0.7654
CAP [18]	13.83	0.7233	14.17	0.7017	14.11	0.6945	16.08	0.7401	15.10	0.7262
Non-Local [19]	17.71	0.7269	18.01	0.7206	17.88	0.7199	18.27	0.7302	18.34	0.7342
GRM [20]	17.03	0.6872	17.11	0.6764	17.19	0.6723	18.08	0.6870	17.98	0.6872
AODnet [27]	18.27	0.7296	18.56	0.7383	18.11	0.7150	18.51	0.7314	18.30	0.7295
GridDehazeNet [30]	21.47	0.8255	22.30	0.8458	22.64	0.8402	22.92	0.8480	21.67	0.8275
Ours	24.89	0.9012	25.36	0.9173	25.29	0.9076	25.45	0.9148	25.13	0.9009

Fig. 10: Results comparison on RESIDE- β [4] dataset.



Fig. 11: Comparison of the intermediate reconstructed result **J** and the final output **C**. The reconstructed image **J** usually contains darker regions. However, the final output **C** recovers the details of the darker regions.

VI. CONCLUSION

We propose a new, large-scale, and diverse dehazing dataset, which contains real outdoor scenes. We select high quality stereo images of real outdoor scenes and render haze on them using depth from stereo pair. Comparing with previous datasets, our dataset is more realistic due to our high-quality depth. We demonstrate that using this proposed dataset greatly improves the dehazing performance on real scenes. In addition, we design a simple physics inspired network model and train it on our proposed dataset. In this way, our approach outperforms other methods by a large margin and is the only one runs at a real time speed. Our dataset is a good complement to existing dehazing dataset and our method provides a practical dehazing solution that are both efficient and effective. We will make the resources available for further dehazing researches.

REFERENCES

- [1] B. T. Nalla, T. Sharma, N. K. Verma, and S. R. Sahoo, "Image dehazing for object recognition using faster rcnn," in *2018 International Joint Conference on Neural Networks (IJCNN)*, 2018, pp. 01–07.
- [2] R. T. Tan, "Visibility in bad weather from a single image," in *IEEE Conference on Computer Vision and Pattern Recognition*, 2008.
- [3] R. Fattal, "Dehazing using color-lines," *ACM Transactions on Graphics*, vol. 34, no. 1, pp. 13:1–13:14, 2014.
- [4] B. Li, W. Ren, D. Fu, D. Tao, D. Feng, W. Zeng, and Z. Wang, "Benchmarking single-image dehazing and beyond," *IEEE Transactions on Image Processing*, vol. 28, no. 1, pp. 492–505, 2019.
- [5] J.-P. Tarel, N. Hautière, L. Caraffa, A. Cord, H. Halmaoui, and D. Gruyer, "Vision enhancement in homogeneous and heterogeneous fog," *IEEE Intelligent Transportation Systems Magazine*, vol. 4, no. 2, pp. 6–20, 2012.
- [6] H. Koschmieder, *Theorie der horizontalen Sichtweite: Kontrast und Sichtweite*. Keim & Nemnich, 1925.
- [7] E. J. McCartney, "Optics of the atmosphere: scattering by molecules and particles," *New York, John Wiley and Sons, Inc., 1976. 421 p.*, vol. 1, 1976.
- [8] Y. Li, S. You, M. S. Brown, and R. T. Tan, "Haze visibility enhancement: A survey and quantitative benchmarking," *Computer Vision and Image Understanding*, vol. 165, pp. 1–16, 2017.
- [9] R. Fattal, "Single image dehazing," *ACM Transactions on Graphics*, vol. 27, no. 3, p. 72, 2008.
- [10] Z. Li, P. Tan, R. T. Tan, S. Z. Zhou, and L.-F. Cheong, "Simultaneous video defogging and stereo reconstruction," in *IEEE Conference on Computer Vision and Pattern Recognition*, 2015.
- [11] S. G. Narasimhan and S. K. Nayar, "Contrast restoration of weather degraded images," *IEEE Transactions on Pattern Analysis and Machine Intelligence*, vol. 25, no. 6, pp. 713–724, 2003.
- [12] J. Kopf, B. Neubert, B. Chen, M. F. Cohen, D. Cohen-Or, O. Deussen, M. Uyttendaele, and D. Lischinski, "Deep photo: Model-based photograph enhancement and viewing," *ACM Transactions on Graphics*, vol. 27, no. 5, pp. 116:1–116:10, 2008.
- [13] Y. Y. Schechner, S. G. Narasimhan, and S. K. Nayar, "Instant dehazing of images using polarization," in *IEEE Conference on Computer Vision and Pattern Recognition*, 2001.
- [14] K. He, J. Sun, and X. Tang, "Single image haze removal using dark channel prior," in *IEEE Conference on Computer Vision and Pattern Recognition*, 2009.
- [15] —, "Single image haze removal using dark channel prior," *IEEE Transactions on Pattern Analysis and Machine Intelligence*, vol. 33, no. 12, pp. 2341–2353, 2011.
- [16] G. Meng, Y. Wang, J. Duan, S. Xiang, and C. Pan, "Efficient image dehazing with boundary constraint and contextual regularization," in *IEEE International Conference on Computer Vision*, 2013.
- [17] K. Tang, J. Yang, and J. Wang, "Investigating haze-relevant features in a learning framework for image dehazing," in *IEEE Conference on Computer Vision and Pattern Recognition*, 2014.
- [18] Q. Zhu, J. Mai, and L. Shao, "A fast single image haze removal algorithm using color attenuation prior," *IEEE Transactions on Image Processing*, vol. 24, no. 11, pp. 3522–3533, 2015.
- [19] D. Berman, T. Treibitz, and S. Avidan, "Non-local image dehazing," in *IEEE Conference on Computer Vision and Pattern Recognition*, 2016.
- [20] C. Chen, M. N. Do, and J. Wang, "Robust image and video dehazing with visual artifact suppression via gradient residual minimization," in *European Conference on Computer Vision*, 2016.
- [21] Y. Li, F. Guo, R. T. Tan, and M. S. Brown, "A contrast enhancement framework with jpeg artifacts suppression," in *European Conference on Computer Vision*, 2014.
- [22] A. Galdran, A. Alvarez-Gila, A. Bria, J. Vazquez-Corral, and M. Bertalmío, "On the duality between retinex and image dehazing," in *IEEE Conference on Computer Vision and Pattern Recognition*, 2018.
- [23] M. Sulami, I. Glatzer, R. Fattal, and M. Werman, "Automatic recovery of the atmospheric light in hazy images," in *IEEE International Conference on Computational Photography*, 2014.
- [24] Y. Li, R. T. Tan, and M. S. Brown, "Nighttime haze removal with glow and multiple light colors," in *IEEE International Conference on Computer Vision*, 2015.
- [25] J. Zhang, Y. Cao, S. Fang, Y. Kang, and C. Wen Chen, "Fast haze removal for nighttime image using maximum reflectance prior," in *IEEE Conference on Computer Vision and Pattern Recognition*, 2017.
- [26] B. Cai, X. Xu, K. Jia, C. Qing, and D. Tao, "Dehazenet: An end-to-end system for single image haze removal," *IEEE Transactions on Image Processing*, vol. 25, no. 11, pp. 5187–5198, 2016.
- [27] B. Li, X. Peng, Z. Wang, J. Xu, and D. Feng, "Aod-net: All-in-one dehazing network," in *IEEE International Conference on Computer Vision*, 2017.
- [28] R. Li, J. Pan, Z. Li, and J. Tang, "Single image dehazing via conditional generative adversarial network," in *IEEE Conference on Computer Vision and Pattern Recognition*, 2018.
- [29] Y. Li, Q. Miao, W. Ouyang, Z. Ma, H. Fang, C. Dong, and Y. Quan, "Lap-net: Level-aware progressive network for image dehazing," in *IEEE International Conference on Computer Vision*, 2019.
- [30] X. Liu, Y. Ma, Z. Shi, and J. Chen, "Griddehazenet: Attention-based multi-scale network for image dehazing," in *IEEE International Conference on Computer Vision*, 2019.
- [31] Y. Liu, J. Pan, J. Ren, and Z. Su, "Learning deep priors for image dehazing," in *IEEE International Conference on Computer Vision*, 2019.
- [32] Y. Qu, Y. Chen, J. Huang, and Y. Xie, "Enhanced pix2pix dehazing network," in *IEEE Conference on Computer Vision and Pattern Recognition*, 2019.
- [33] W. Ren, S. Liu, H. Zhang, J. Pan, X. Cao, and M.-H. Yang, "Single image dehazing via multi-scale convolutional neural networks," in *European Conference on Computer Vision*, 2016.
- [34] W. Ren, L. Ma, J. Zhang, J. Pan, X. Cao, W. Liu, and M.-H. Yang, "Gated fusion network for single image dehazing," in *IEEE Conference on Computer Vision and Pattern Recognition*, 2018.
- [35] D. Yang and J. Sun, "Proximal dehaze-net: a prior learning-based deep network for single image dehazing," in *European Conference on Computer Vision*, 2018.
- [36] H. Zhang and V. M. Patel, "Densely connected pyramid dehazing network," in *IEEE Conference on Computer Vision and Pattern Recognition*, 2018.

- [37] M. Pharr and G. Humphreys, *Physically based rendering: From theory to implementation*. Morgan Kaufmann, 2010.
- [38] C. Sakaridis, D. Dai, and L. Van Gool, "Semantic foggy scene understanding with synthetic data," *International Journal of Computer Vision*, vol. 126, no. 9, pp. 973–992, 2018.
- [39] M. Cordts, M. Omran, S. Ramos, T. Rehfeld, M. Enzweiler, R. Benenson, U. Franke, S. Roth, and B. Schiele, "The cityscapes dataset for semantic urban scene understanding," in *IEEE Conference on Computer Vision and Pattern Recognition*, 2016.
- [40] N. Silberman, D. Hoiem, P. Kohli, and R. Fergus, "Indoor segmentation and support inference from rgb-d images," in *European Conference on Computer Vision*, 2012.
- [41] D. Scharstein and R. Szeliski, "High-accuracy stereo depth maps using structured light," in *IEEE Conference on Computer Vision and Pattern Recognition*, 2003.
- [42] F. Liu, C. Shen, G. Lin, and I. Reid, "Learning depth from single monocular images using deep convolutional neural fields," *IEEE Transactions on Pattern Analysis and Machine Intelligence*, vol. 38, no. 10, pp. 2024–2039, 2015.
- [43] F. Liu, C. Shen, and G. Lin, "Deep convolutional neural fields for depth estimation from a single image," in *IEEE Conference on Computer Vision and Pattern Recognition*, 2015.
- [44] *pyscenedetect*, <https://pyscenedetect.readthedocs.io/>.
- [45] B. Zhou, H. Zhao, X. Puig, T. Xiao, S. Fidler, A. Barriuso, and A. Torralba, "Semantic understanding of scenes through the ade20k dataset," *International Journal of Computer Vision*, 2018.
- [46] D. Sun, X. Yang, M.-Y. Liu, and J. Kautz, "PWC-Net: CNNs for optical flow using pyramid, warping, and cost volume," in *IEEE Conference on Computer Vision and Pattern Recognition*, 2018.
- [47] Y. Li, D. Min, M. N. Do, and J. Lu, "Fast guided global interpolation for depth and motion," in *European Conference on Computer Vision*, 2016.
- [48] D. Ulyanov, A. Vedaldi, and V. S. Lempitsky, "Instance normalization: The missing ingredient for fast stylization," *CoRR*, vol. abs/1607.08022, 2016. [Online]. Available: <http://arxiv.org/abs/1607.08022>
- [49] J. Johnson, A. Alahi, and L. Fei-Fei, "Perceptual losses for real-time style transfer and super-resolution," in *European Conference on Computer Vision*, 2016.
- [50] K. Simonyan and A. Zisserman, "Very deep convolutional networks for large-scale image recognition," in *International Conference on Learning Representations*, 2015.
- [51] O. Russakovsky, J. Deng, H. Su, J. Krause, S. Satheesh, S. Ma, Z. Huang, A. Karpathy, A. Khosla, M. Bernstein, A. C. Berg, and L. Fei-Fei, "ImageNet Large Scale Visual Recognition Challenge," *International Journal of Computer Vision*, vol. 115, no. 3, pp. 211–252, 2015.
- [52] D. P. Kingma and J. Ba, "Adam: A method for stochastic optimization," in *International Conference on Learning Representations*, 2015.
- [53] Q. Huynh-Thu and M. Ghanbari, "Scope of validity of psnr in image/video quality assessment," *Electronics Letters*, vol. 44, no. 13, pp. 800–801, June 2008.
- [54] Z. Wang, A. C. Bovik, H. R. Sheikh, and E. P. Simoncelli, "Image quality assessment: from error visibility to structural similarity," *IEEE Transactions on Image Processing*, vol. 13, no. 4, pp. 600–612, April 2004.



Ruoteng Li received the B.S. degree from National University of Singapore, Singapore, in 2013 and received his Ph.D degree from electrical and computer engineering, National University of Singapore in 2020.



Xiaoyi Zhang Xiaoyi Zhang received the B. S. degree from Sun Yat-Sen University, Guangzhou, China, in 2011, and the Ph.D. degree from the National University of Singapore, Singapore, in 2018. Her current research interests include artificial intelligence and robotics.



Shaodi You is an Assistant Professor at University of Amsterdam (UvA), Netherlands. He receives his Ph.D. and M.E. degrees from The University of Tokyo, Japan in 2015 and 2012 and his bachelor's degree from Tsinghua University, P. R. China in 2009. His research interests are 1. physics based vision, 2. perception based vision and learning, and 3. 3D geometry. He is best known for his work on visual enhancement for rainy days. He is an area chair for ECCV2020, He is a program chair for ICCV2017, ICCV2019 Workshop on Physics Based Vision meets Deep Learning. He is a program chair for ICCV2019 Workshop on e-Heritage. He is a general chair for DICTA2018.



Yu Li received his Ph.D. degree from School of Computing, National University of Singapore in 2015. He is a Senior Research Scientist at Tencent PCG Applied Research Center. He also holds a Research Affiliate with University of Illinois at Urbana-Champaign (UIUC). He was a postdoc researcher at UIUC Advanced Digital Sciences Center. His research interests include computer vision, computational photography, and computer graphics. He is the winner of Singapore IDA Medal 2016. He is a program chair for ICCV2017, ICCV2019 Workshop on Physics Based Vision meets Deep Learning.